ISSN 1343-2230
CNS-REP-65
December, 2004

CNS-REP-65

CNS Report

FERMI
FEB 3 2005
LIBRARY

Proton Polarizing system with Ar-ion laser for $\vec{p}$-RI scattering experiments

T. Wakui, M. Hatano, H. Sakai, T. Uesaka, A. Tamii

Submitted to Nucl. Instr. and Meth. A

Center for Nuclear Study (CNS)

Graduate School of Science, the University of Tokyo
Wako Branch at RIKEN, 2-1 Hirosawa, Saitama 351-0198, Japan
Correspondence: cnsoffice@cns.s.u-tokyo.ac.jp

Proton polarizing system with Ar-ion laser for $\vec{p}$-RI scattering experiments

T. Wakui [a,*], M. Hatano [b,c,1], H. Sakai [a,b], T. Uesaka [a], A. Tamii [d]

[a] *Center for Nuclear Study, University of Tokyo, 7-3-1 Hongo, Bunkyo, Tokyo 113-0033, Japan*

[b] *Department of Physics, University of Tokyo, 7-3-1 Hongo, Bunkyo, Tokyo 113-0033, Japan*

[c] *RIKEN, 2-1 Hirosawa, Wako, Saitama 351-0198, Japan*

[d] *Research Center for Nuclear Study, Osaka University, 10-1 Mihogaoka, Ibaraki, Osaka 567-0047, Japan*

Abstract

A proton polarizing system for use in scattering experiments with radioactive isotope beams is described. Protons in a naphthalene crystal doped with pentacene are polarized in a magnetic field of 0.3 T at 100 K by transferring a large population difference among the photo-excited triplet states of pentacene to the hydrogen nuclei. An Ar-ion laser, which demands minimal maintenance during scattering experiments, is employed to excite the pentacene molecules. A proton polarization of 37% is obtained.

Key words: Polarized target; Aromatic molecules; Unstable nuclei
PACS: 29.25.Pj; 76.70.Fz; 33.40.+f

1 Introduction

Radioactive isotope (RI) beams have dramatically extended research in nuclear physics to include nuclei that are far from the β-stability line. A lot of information on nuclear structure of unstable nuclei should be obtained by measuring the scattering of an RI beam from a polarized proton target. The present study is aimed at taking the first step towards this direction by constructing a polarized target that can be used in RI beam experiments.

In the RI beam experiments, a high-density target is necessary for sufficient luminosity since the intensity of the RI beams is typically as low as $<10^6$ particles/s [1]. In this respect, a solid target, rather than a gas target, is desirable. The nucleus of hydrogen atom in a solid material can be a polarized proton target. Protons in solid material are typically polarized in a magnetic field of 2 T or higher and at a sub-Kelvin temperature by utilizing highly polarized electrons under these conditions [2,3]. Although these conditions provide proton polarizations of more than 80%, the detection of low energy recoiled protons, typically 10 MeV, is severely limited. The strong magnetic field prevents the recoiled pro-

* Corresponding author.
Email address:
wakui@cns.s.u-tokyo.ac.jp (T. Wakui).
[1] Present address: Central Research Laboratory, Hitachi Ltd., Tokyo 185-8601, Japan

tons from reaching a detector.

One candidate for a target applicable to the RI beam experiments is a "frozen spin" target, which can operate in a reduced magnetic field around 0.3 T after polarizing protons [2,3]. Another candidate is a target that uses a crystal of aromatic molecules such as naphthalene doped with pentacene. We adopted the latter for $\vec{p}$-RI scattering experiments. Protons in the crystal can be polarized under a low magnetic field and at a high temperature by combining methods called "microwave-induced optical nuclear polarization" (MIONP) and "integrated solid effect"(ISE) [4]. In the MIONP, pentacene molecules are optically pumped to the photo-excited triplet state. In the triplet state, a large population difference of 73% among the Zeeman sublevels spontaneously appears [5,6]. The population difference does not depend on the magnetic field strength or the temperature. Protons are polarized even at 0.3 T and 100 K by transferring the population difference to the protons using the cross-relaxation between electrons and protons, which was originally called ISE [4,7].

Several groups have applied this novel technique to polarize protons [4,8,9]. Pentacene molecules have been excited with a nitrogen laser [4,8] and recently with a flashlamp-pumped dye laser [9,10]. The optimal wavelength to excite pentacene is around 600 nm and the dye laser can be tuned to that wavelength, but it is not suited for $\vec{p}$-RI scattering experiments due to the short lifetime of the dye [11]. The procedure to change the dye interrupts the measurement and the polarizing process for a few hours every day. Moreover, the flashlamp-pumped dye laser is commercially unavailable recently. Therefore, we decided to use another type of laser, an Ar-ion laser, which demands less maintenance during the experiment.

To establish a polarized target that can be applied to the experiments with RI beams, we studied the effectiveness of an Ar-ion laser as a light source for the optical excitation with a newly constructed proton polarizing system. In this paper, we describe the design and operation of the proton polarizing system and the results of the proton polarization using the Ar-ion laser. In Section 2, principles of a proton polarizing system are briefly presented. Section 3 deals with the procedure for refining and crystallizing the target material. The proton polarizing system is described in Section 4. In Section 5, the laser system and its operation are given. The optimization of the experimental conditions such as the direction of the long molecular axis, magnetic field strength, and microwave power are explained in Section 6. Then the results of proton polarization and relaxation are presented in Section 7 and the Summary follows.

2 Principle of the proton polarizing system

Protons in a naphthalene crystal doped with pentacene are polarized by repeating a three-step process: optical excitation, polarization transfer, and polarization diffusion. Below is a brief description of the optical excitation and the polarization transfer.

2.1 Optical excitation

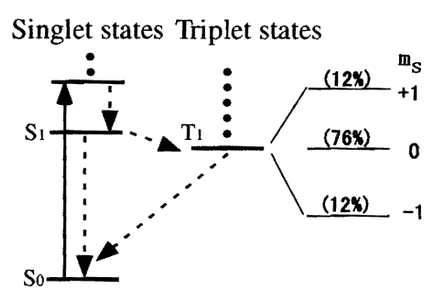

Fig. 1. Excitation scheme of a pentacene molecule. Pentacene molecules are excited in higher singlet states by irradiating with a laser and a part of the pentacene molecules decay to the lowest triplet state and a large population difference is spontaneously produced. The initial populations of the sublevels just after initiating excitation are shown in parentheses. The population difference is transferred to protons by a cross-relaxation method.

The first step in polarizing protons is to produce a population difference among the magnetic sublevels in the photo-excited triplet state of the pentacene molecules using a pulsed laser beam. Figure 1 shows the excitation scheme of pentacene molecules. Pentacene molecules are excited by laser irradiation to higher singlet states and decay to the first excited singlet state, S_1, in several picoseconds. Most of pentacene molecules in the S_1 state decay to the ground state, S_0, but a small fraction of them decay into the lowest triplet state, T_1. The transition from S_1 to T_1, the so-called intersystem crossing (ISC), occurs due to spin-orbit coupling, which mixes the singlet and triplet states. The branching ratio from S_1 to T_1, the so-called ISC yield, is as small as a few % at approximately 2 K [12,13]. The ISC yield should increase as the temperature increases, but is still much smaller than unity at 100 K. In a magnetic field, a population difference spontaneously appears among the Zeeman sublevels of the T_1 state. The maximum degree of the population difference appears when the external magnetic field is applied parallel to the long molecular axis of pentacene [5,6]. In this case, the populations of sublevels are 12%, 76%, and 12% for $m_s=-1$, 0, and +1, respectively. The population difference between the $m_s=-1$ and 0 sublevels is 73%. Pentacene molecules in the sublevels of the T_1 state decay back to the S_0 state. The lifetime of the $m_s=0$ sublevel is 26 μs, while that of the $m_s=-1$ sublevel has a longer lifetime, 83 μs [14].

2.2 Polarization transfer

Before pentacene in the T_1 state decays back to the S_0 state, the population difference is transferred to protons by means of cross-relaxation. In the cross-relaxation technique, a magnetic field is adiabatically swept over the region of relevant ESR lines in the T_1 state in the presence of the pulsed microwave irradiation. The effective Larmor frequency, ω_{eff}, in a coordinate system rotating with a frequency of ω can be written as

$$\omega_{\mathrm{eff}} = \sqrt{(\omega_{\mathrm{s}} - \omega)^2 + \omega_{\mathrm{R}}^2}\ , \qquad (1)$$

where ω_{s} is the Larmor frequency of electrons and ω_{R} is the Rabi frequency. The Rabi frequency, $\omega_{\mathrm{R}} = \gamma_{\mathrm{s}} H_1$, is a product of the gyromagnetic ratio, γ_{s}, and the amplitude of the oscillating magnetic field, H_1, created by the microwave. When the resonance condition is satisfied, $\omega = \omega_{\mathrm{s}}$, ω_{eff} depends only on H_1. Thus, adjusting H_1 can tune ω_{eff} to the Larmor frequency of protons, ω_{I}. Here the polarization transfer from the electrons to protons occurs due to the dipolar interaction between them. This is the Hartmann-Hahn condition for cross-relaxation. In addition, by sweeping the magnetic field over the ESR line, all of the "spin packets" in the line constructively contribute to the polarization transfer [7]. Through this technique, the population difference can efficiently be transferred to protons even in a low magnetic field where the conventional DNP method does not work well due to an unresolved ESR line [3].

3 Fabrication of target crystal

A crystal of naphthalene doped with 0.01 mol% pentacene is the target material. The crystal is fabricated by a vertical Bridgman method after refining the naphthalene powder.

3.1 Refinement

Paramagnetic impurities contained in a crystal cause the relaxation of proton spins [15]. Commercially available naphthalene powder contains approximately 1% impurities, which is about 100 times greater than the pentacene concentration, 0.01 mol%. Since the small relaxation rate of proton spins is indispensable for obtaining a higher proton polarization, the powder is refined by the

zone-melting method to reduce impurities to a level less than the pentacene concentration.

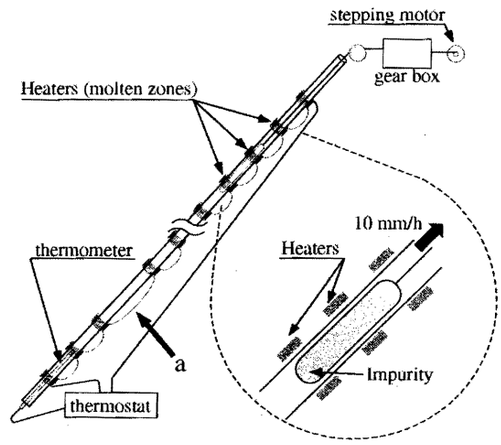

Fig. 2. Schematic drawing of the zone-melting apparatus. The starting position of the zone-melting process is indicated by "a". A stepping motor, a gearbox, pulley wheels, and a wire are used to pull up the glass tube.

The zone-melting apparatus, shown in Fig. 2, contains a glass tube (16 mm in diameter, 2400 mm long) equipped with 16 molten zones at 80 mm intervals. The molten zones are heated by 7 turns of Nichrome wires wound around the glass tube. Three additional heaters are equipped at the lowest portion of the glass tube. To monitor the temperature, a platinum resistance thermo-sensor is placed inside the additional heaters. The temperature is maintained at 360 K, which is 7 K higher than the melting point of naphthalene. The glass tube is tilted approximately 45 degrees to prevent bubbles from forming at a boundary layer between the liquid and solid phases.

A glass ampoule containing naphthalene powder is pulled at a rate of 10 mm/h through the glass tube. In the molten zones, the impurities are separated from naphthalene due to the segregation effect and are concentrated in the lower part of the ampoule. The procedure is repeated more than three times so that the naphthalene powder passes more than 40 molten zones. After this process, the refined naphthalene is removed from the ampoule and mixed with pentacene powder with a mole ratio of 1:0.0001. The mixed powder is then enclosed in a glass ampoule for crystallization.

3.2 Crystallization

The material is crystallized using the vertical Bridgman method. In this method, two

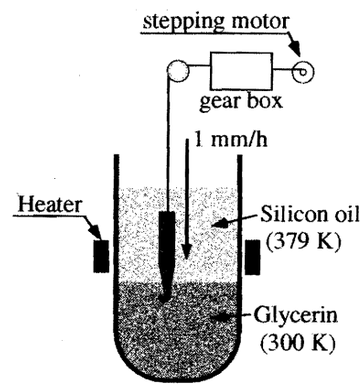

Fig. 3. A schematic view of the apparatus for the Bridgman method. Silicon oil is used to produce the zone above the melting temperature of naphthalene, while glycerin produces the zone below it. The travel mechanism is essentially the same as the refinement apparatus.

temperature-zones are prepared: one above and the other below the melting temperature of naphthalene, 353 K. The mixed powder in the ampoule is moved downward from the zone above the melting point to the zone below it. Crystallization occurs as the temperature of the mixed powder slowly decreases between the two zones.

To create an appropriate temperature gradient, we used silicon oil and glycerin for high and low temperature zones, respectively, as shown in Fig. 3. A glass vessel, which contains silicon oil and glycerin, is used as a "furnace" to grow the crystal. A heater that consists of 30 turns of Nichrome wire is wound at the upper portion of the vessel, and heats up the silicon oil to a temperature of 379 K. A platinum resistance thermo-sensor monitored and a thermostat controlled the temperature of the silicon oil. Figure 4 shows the measured temperature distribution around the boundary between the silicon oil and the glycerin. In this figure, the boundary

is the origin of the position in the glass vessel. A temperature gradient of 1.4 K/mm is formed around the position where the temperature corresponds to the melting point of naphthalene.

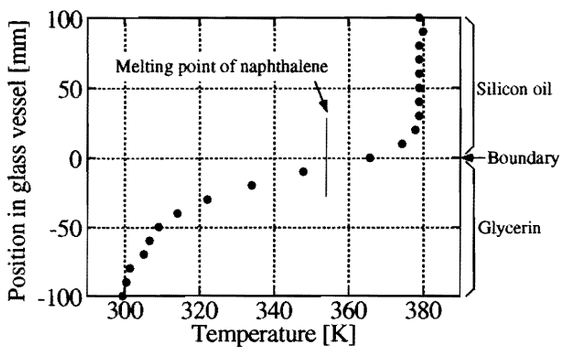

Fig. 4. Temperature distribution around the boundary between the silicon oil and glycerin. The boundary is the origin of the position in the glass vessel.

The glass ampoule that contains the mixed powder has an inner diameter of 18 mm and a length of 150 mm. The glass ampoule is initially placed in the high-temperature zone. After the powder is molten, the glass ampoule is lowered at a rate of 1 mm/h. Near the boundary between the silicon oil and the glycerin, crystallization continuously occurs upward from the bottom of the glass ampoule. A sample piece used in a polarization experiment is cut from the fabricated crystal.

To confirm the quality of the refinement and the crystallization, the relaxation time of proton polarization is a good indicator. The results are described in Section 7.

4 Proton polarizing system

The proton polarizing system, shown in Fig. 5, consists of a C-type magnet that produces an external magnetic field, an Ar-ion laser for optical excitation, a microwave system for polarization transfer, and an NMR system that measures proton polarization. Each system is described in the following subsections, except the Ar-ion laser, which is described in Section 5. The target crystal is mounted in a TE_{011} cylindrical cavity placed in the C-type magnet.

4.1 Magnet

The C-type magnet has a pole diameter of 120 mm. The gap between the poles is 60 mm. At the center of the return yoke, a hole with 40 mm diameter is bored for the path of a laser beam. The magnet produces a maximum magnetic field of 0.4 T. A field non-uniformity measured with an NMR teslameter at 0.3 T is smaller than 3.5×10^{-4} over a spherical volume of 20 mm diameter. The non-uniformity of the external field is sufficiently smaller than the internal field of a naphthalene crystal. Note that the naphthalene crystal has an internal field of approximately 2 mT, which is a fraction, 7×10^{-3}, of the external field, 0.3 T.

4.2 Microwave cavity

A TE_{011} cylindrical microwave cavity, in which a target sample is mounted, is used to produce an oscillating field for the polarization transfer. The resonance frequency of the cavity is 9.1 GHz. The loaded Q of the cavity is approximately 4000 at room temperature. The cavity facilitates the magnetic field sweep for the polarization transfer and the laser irradiation for optical excitation. Figure 6(a) and (b) show cross- and longitudinal-sectional views of the cavity, respectively.

A set of field modulation coils is used for the magnetic field sweep. The coils are configured in a six-loop arrangement and are made of twelve Cu rods that are 1.5 mm in diameter. The coils are installed in the cavity parallel to the cylinder axis of the cavity, as shown in Fig. 6. This coil configuration enables laser irradiation to the target sample without losing the Q of the cavity. The magnetic field sweep is achieved by applying a triangular current, which is supplied by

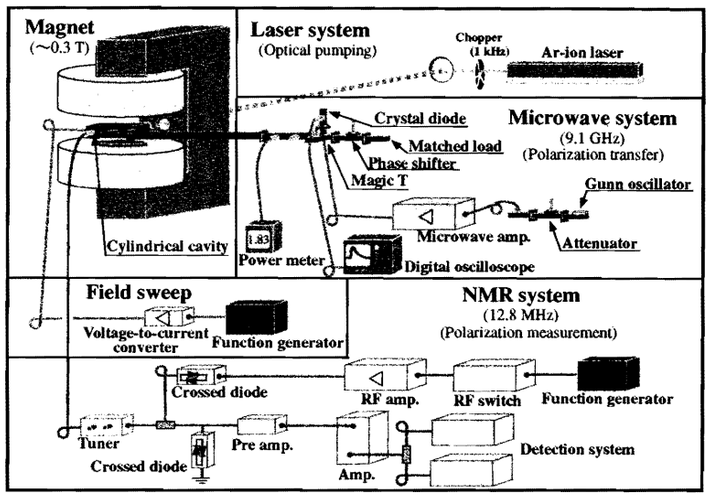

Fig. 5. A schematic view of the proton polarizing system. The system consists of a magnet, a laser for optical excitation, a microwave system for polarization transfer, and an NMR system for polarization measurements.

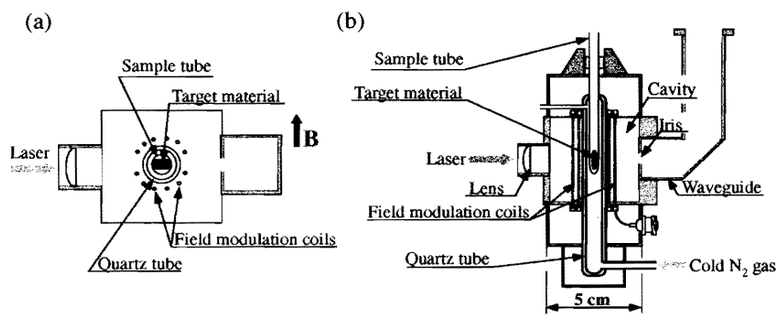

Fig. 6. Cross-sectional (a) and longitudinal-sectional (b) views of the cylindrical cavity. The resonance frequency and loaded Q are 9.1 GHz and 4000, respectively.

a high-power operational amplifier, to the field modulation coils (see Fig. 17).

The cavity has an optical window for the laser irradiation. A 20 mm diameter lens is used as the optical window to focus the laser beam on the target sample. The position of the lens can be adjusted to produce an appropriate spot size of the laser beam on the target sample. To prevent water condensation when the target sample is maintained at a low temperature, dry nitrogen gas is blown on the lens.

The target sample in the cavity is cooled to a desired temperature between 77 K and room temperature, depending on the purpose of experiment. A sample tube in which the target sample is mounted is inserted into a double walled and vacuum insulated quartz tube. The target sample is cooled by cold nitrogen gas introduced inside the quartz tube (see Fig. 6). The temperature of the target sample, which is controlled by adjusting the flow rate of the cold nitrogen gas, is measured with a CA thermocouple.

4.3 Microwave circuit

Figure 7 shows a schematic diagram of the microwave system used for the polarization transfer. The microwaves are generated by a Gunn oscillator with a varactor modulator. The maximum output power is 80 mW. Microwaves are then pulsed and amplified by a solid-state amplifier, whose maximum output power is 20 W. The

typical operating power is around 2 W, determination of which is described in Section 6. The pulsed microwave is split into arms 2 and 3 of a magic-T. Arm 3 is connected to a phase shifter with a terminator. Microwaves from arm 2 reach the cavity through a directional coupler. The transmitted power to the cavity is monitored by a power meter attached to the directional coupler. A coupling iris adjusts the coupling between the cavity and the waveguides. The reflected microwaves from the cavity are detected by a crystal detector attached to arm 4 of the magic-T. The detected signal is used for several purposes: to adjust the coupling iris, to tune the microwave frequency to match the resonant frequency of the cavity, and to observe a time-resolved ESR signal of the lowest triplet state of pentacene.

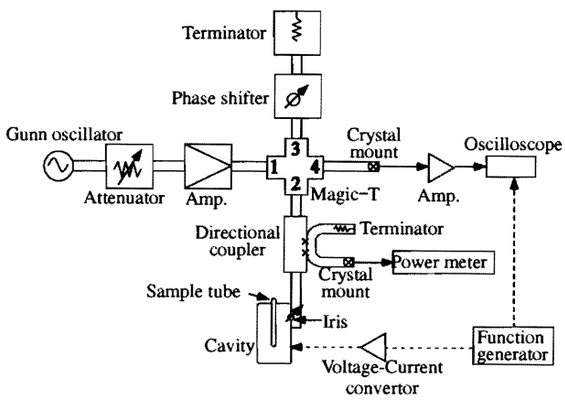

Fig. 7. Block diagram of the microwave circuit.

4.4 NMR system

The proton polarization is measured with a pulsed NMR spectrometer, which is schematically shown in Fig. 8. The frequency of NMR is 12.8 MHz at a magnetic field of 0.3 T. A continuous-wave RF signal generated by a synthesizer is formed into an RF pulse and is amplified by a power amplifier with a maximum output power of 500 W. After passing through a crossed diode and a tuner, the amplified RF signal is transmitted to a 8-turn NMR coil. The Q of the NMR coil is set to 15 in order to reduce the dead-time of the detection system due to a strong RF pulse.

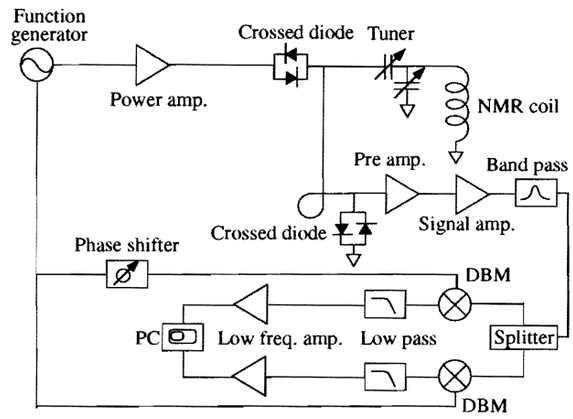

Fig. 8. Block diagram of the NMR system.

A signal induced in the NMR coil after irradiating with a pulsed RF signal is amplified with a preamplifier that has a 30 dB gain. In order to reduce the noise from the power amplifier, the detection system is decoupled from the power amplifier by crossed diodes. The NMR signal is further amplified with a signal amplifier and is then passed through a bandpass filter. To accomplish quadrature detection, two double balanced mixers (DBMs) are used with reference signals that are 90 degree out of phase with each other. The resulting signal is processed by a lowpass filter and a low-frequency amplifier so that only the lower frequency component is recorded.

To avoid destruction of the proton polarization in the polarization buildup process, the NMR measurement is performed using a weak RF pulse instead of a 90 degree pulse. The power of the weak pulse is adjusted so that the polarization destruction is less than 0.3% of proton polarization. The measured NMR signals are calibrated by comparing them to the NMR signal measured at thermal equilibrium (TE).

The NMR signal at TE is measured using a 90 degree pulse since the signal is very small due to the small proton polarization, 3×10^{-6}, at 0.3 T at 100 K. The difference in sensitivity between the weak pulse and the 90 degree pulse methods

is calibrated by comparing the NMR signals obtained using the two methods at several polarizations between 0.01% and 1%.

To ensure the validity of the calibration method, the NMR system must have linearity over a dynamic range of more than 10^4. The linearity of the NMR system is experimentally verified with an additional transmitter coil that is set into the sample tube placed at the target position. Figure 9 shows the result of the measurement that clearly shows that the NMR system has the linearity over the measured range spanning 10^4 in amplitude. The range can be safely extended to 10^5 by adjusting the gain of the receiver. The error in the polarization due to the uncertainty of the linearity is 1.5%.

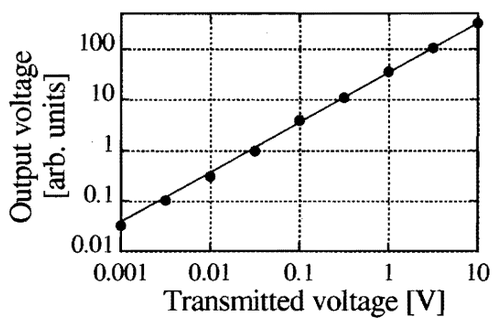

Fig. 9. Result of the linearity measurement.

The uncertainty of measured polarization is dominated by the uncertainty in the amplitude of the TE signal. The amplitude of the TE signal is too small even at a 90 degree pulse to achieve a sufficient signal-to-noise ratio. Thus, the TE signals must be accumulated by repeating the measurements. However, a 90 degree pulse saturates the resonance and more than three days are necessary to reach TE again due to the long relaxation time of protons. This fact limits the number of repetitions for acquiring TE signals. Therefore, the accuracy of the polarization is typically as much as 10%.

The polarization uncertainty includes errors due to magnetic field strength measurements and temperature in determining the proton polarization at TE. The magnetic field strength is measured with a Hall probe calibrated by the NMR frequency of protons in water. The error of the field strength measurement mainly comes from the uncertainty in the calibration constant and is 0.3%. The error from the temperature measurement is caused by the temperature fluctuation due to the instability of the flow rate of cold nitrogen gas and is estimated to be 2.5%.

5 Laser system and operation

For the optical excitation, an Ar-ion laser (Coherent TSM25) with a standard power specification for the wavelength ranging from 454.5 to 528.7 nm and the total maximum power of 25 W in the multiline operation mode is used. The operation mode of the laser can easily be changed between the multiline and the single-line modes. Among the available wavelengths of an Ar-ion laser, the preferred wavelength for the excitation of pentacene is 514 nm since pentacene has a local absorption maximum near 514 nm as shown in Fig. 10. This figure shows the absorption spectrum of pentacene in a naphthalene crystal measured with a spectrophotometer (StellarNet EPP2000). To achieve a pulsed laser beam from a cw laser beam, an optical chopper with two chopper blades is used. The pulse width can be changed by rotating one blade with respect to the other.

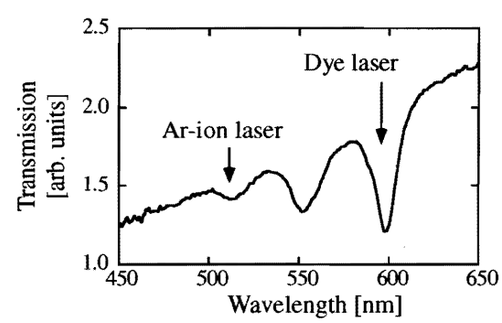

Fig. 10. Absorption spectrum of pentacene in a naphthalene crystal. The spectrum is measured with a spectrophotometer (StellarNet EPP2000).

The pulse width is a compromise between the

population of the T_1 state and the population difference. The population of the T_1 state affects the efficiency of the polarization transfer while the population difference determines the upper limit of proton polarization. In order to understand how the population of the T_1 state and the population difference depend on the pulse width, we consider a simple model for calculating the populations ρ_i for the sublevels in the T_1 state as a function of the pulse width. Here i stands for the sublevels: "−" for m_s=−1, "0" for m_s=0, and "+" for m_s=+1.

We start with the following equation:

$$\frac{d\rho_i}{dt} = k_{1i}\ \rho_s - k_{2i}\ \rho_i. \tag{2}$$

Here ρ_i and ρ_s are the sublevel populations of the T_1 state and the S_1 state, respectively, and k_{1i} and k_{2i} are the transition rates for the $S_1 \rightarrow T_1$ and $T_1 \rightarrow S_0$ transitions, respectively. The transition rate, k_{1i}, is related to the lifetime of S_1 state, τ_s, and can be written as $k_{1i} = (YC_i)/\tau_s$, where Y is the ISC yield described in Section 2 and C_i is the initial population for each sublevel just after beginning the excitation. The transition rate, k_{2i}, is given by $k_{2i} = 1/\tau_i$, where τ_i is the lifetime of each sublevel. In general, the population of the S_1 state, ρ_s, depends on time if the number of photons is sufficient to deplete pentacene in the S_0 state. However, under the present conditions, the photon number, 5×10^{11}, in a period of the lifetime of S_1 state, 20 ns, is too small compared with the pentacene number of 10^{16}. In addition, the ISC yield is very small. Consequently, most of excited pentacene decays back to the S_0 state. Thus, we can approximate that ρ_s is constant during laser irradiation. The populations of the sublevels ρ_i are then derived from Eq. (2) as

$$\rho_i = \frac{k_{1i}}{k_{2i}}\ \rho_s\ \{1 - \exp(-k_{2i}\ t)\} \tag{3}$$

$$= \frac{YC_i}{\tau_s}\tau_i\rho_s\{1 - \exp(-\frac{1}{\tau_i}t)\}. \tag{4}$$

Table 1
Parameters used to calculate the population.

Parameter	value	Ref.
τ_s	19.5 ns	[16]
τ_0	26 μs	[14]
τ_-	83 μs	[14]
C_0	0.76	[6]
C_-	0.12	[6]

Since ρ_s is assumed constant, the relative population ρ_i/ρ_s ($\equiv \rho'_i$) is used in the following calculation.

The sublevels related to the polarization transfer are the m_s=0 and −1 sublevels. The sum of the relative populations of the sublevels, $\rho'_T = \rho'_0 + \rho'_-$, is calculated to estimate the population in the T_1 state. Figure 11 shows the result of the calculation. Table 1 lists previously reported values of lifetimes and initial populations used. The assumed ISC yield, Y, is 2%. The results show that the population of the T_1 state gradually increases during laser irradiation and accordingly a longer pulse width is better for increasing the number of pentacene molecules that contribute to the polarization transfer.

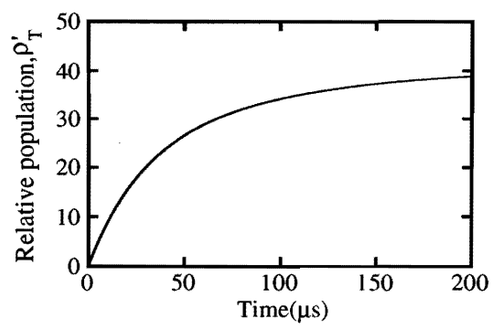

Fig. 11. Time dependence of the sum of the relative populations. The sublevels related to the polarization transfer are m_s=0 and −1 and the sum of the relative populations is $\rho'_T = \rho'_- + \rho'_0$.

To estimate the population difference between the m_s=0 and −1 states, we calculate the normalized population difference, $P_e = (\rho'_0 - \rho'_-)/(\rho'_0 + \rho'_-)$. Figure 12 shows the calculated results. The parameters used in this

calculation are the same as that of ρ'_T. The results show that the population difference gradually decreases while irradiating with the laser due to the shorter lifetime of m_s=0 than that of m_s=−1. Since the population difference determines the upper limit of proton polarization, a shorter pulse width is better for a higher proton polarization.

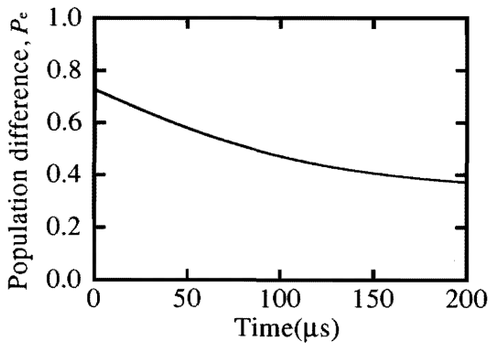

Fig. 12. Calculated population difference, P_e, as a function of time. The population difference between m_s=0 and −1 is defined as $P_e = (\rho'_0 - \rho'_-)/(\rho'_0 + \rho'_-)$.

Figures 11 and 12 show that there is an optimal pulse width for a high proton polarization. To find the optimal pulse width, a "figure of merit" (FOM) defined as $P_e\rho'_T$ is calculated and the result is shown in Fig. 13. From this figure, the optimal pulse width is 80 μs.

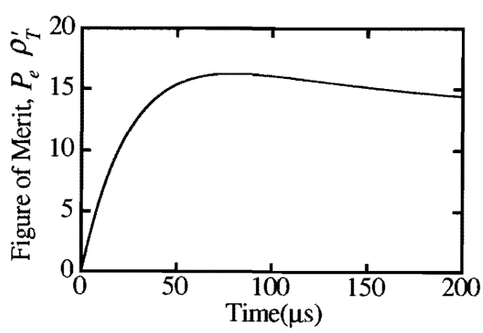

Fig. 13. Figure of merit, $P_e\rho'_T$. The optimal pulse width is 80 μs.

The conclusion by the simple model should be modified when it is applied to an actual case due to the unexpected effect by laser irradiation on the relaxation rate of proton polarization. The relaxation rate increases from 0.049 to 0.12 h^{-1} after laser irradiation with an integrated energy of 11 W·h. Although the irradiation effect on the relaxation rate is not well understood, it can be assumed that the irradiation effect increases as the pulse width increases. A longer pulse width increases the efficiency of polarization transfer, but also increases the relaxation rate of proton polarization. The increase of the relaxation rate will decrease the attainable proton polarization. Therefore, we conservatively determined a pulse width of 20 μs in order to keep the increase in the relaxation rate below 5% during the experiment. The irradiation effect will be investigated in more detail in the near future.

6 Optimization of experimental condition

To attain a high proton polarization, experimental conditions such as the direction of the long molecular axis of pentacene, magnetic field strength, and microwave power should be optimized.

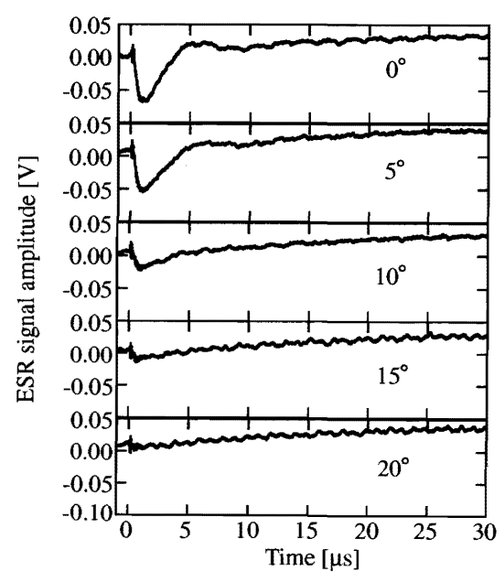

Fig. 14. Time-resolved ESR spectrum of pentacene. Angles shown in the figure indicate the angles of the long molecular axis with respect to the magnetic field.

To obtain a large population difference in the lowest triplet state, the long molecular axis of pentacene should be parallel to the magnetic field [6]. The direction of the long molecular axis can be adjusted by observing the double refraction and by finding the cleavage surface. Coarse adjustment of the axis was conducted by monitoring the amplitude, which is proportional to the population difference, of the time-resolved ESR signal of pentacene in the T_1 state. Figure 14 shows the observed ESR signal obtained by changing the angle between the long molecular axis and the magnetic field at 5 degree intervals. In this measurement, a Nd:YAG laser with a maximum energy of 100 mJ was used instead of an Ar-ion laser since the chopped beam of an Ar-ion laser, 200 μJ, is too weak to observe the ESR signal.

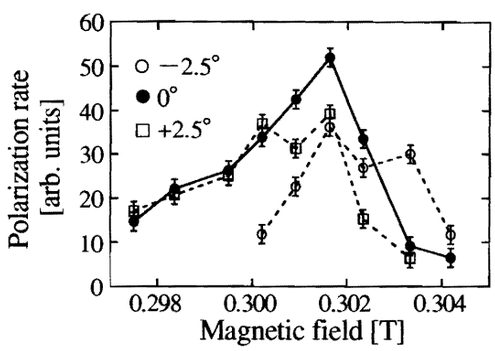

Fig. 15. The polarization rate as a function of the field strength for each angle. The amplitude measured after polarizing protons for 5 minutes is used as the polarization rate.

Fine adjustment of the axis was conducted by maximizing the polarization rate, dP_p/dt, which can be estimated by observing the NMR signal after polarizing protons for 5 minutes. The proton polarization, P_p, during the polarization buildup can be written as [8]

$$P_p = \frac{A\overline{P_e}}{A+\Gamma}\{1-\exp[-(A+\Gamma)t]\}, \tag{5}$$

where $\overline{P_e}$ is the average population difference in the T_1 state, A is the buildup rate that is proportional to the efficiency of polarization transfer from electron to proton, and Γ is the total relaxation rate. For $(A+\Gamma)t \ll 1$, the polarization rate derived from Eq. (5) reduces to

$$\frac{dP_p}{dt} = A\overline{P_e}. \tag{6}$$

Thus, the polarization rate is approximately proportional to the population difference and the buildup rate as long as $(A+\Gamma)t \ll 1$. In the present experiment, $(A+\Gamma)t$ is always less than 0.04.

Figure 15 shows an example of polarization rate as a function of the magnetic field strength for angles of −2.5, 0, and +2.5 degrees between the long molecular axis and the magnetic field. The maximum polarization rate decreases by more than 20% when the angle of the long molecular axis is shifted by 2.5 degrees with respect to the magnetic field direction. Thus, the crystal orientation is essential for a high proton polarization.

Optimization of the microwave power is equally important. The microwave power should be adjusted to fulfill the Hartmann-Hahn condition for the cross-relaxation as described in Section 2. Figure 16 shows the dependence of the polarization rate on the microwave power. The polarization rate rapidly increases with the microwave power and reaches a maximum at 1.8 W. Above 2 W, the Hartmann-Hahn condition can not be fulfilled. $\omega_{\rm eff}$ is always higher than $\omega_{\rm I}$ during the magnetic field sweep. Therefore, the polarization rate decreases with a microwave power. From Fig. 16, the microwave power was chosen to be 1.8 W.

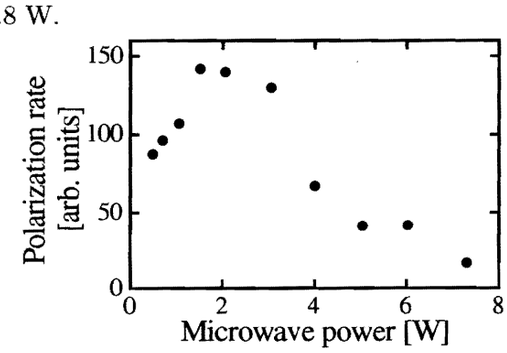

Fig. 16. NMR signal amplitude as a function of microwave power for the polarization transfer. The most appropriate power for polarizing protons is 1.8 W.

Table 2
Parameters used in the polarizing experiment.

Magnetic field	0.3 T
Temperature	100 K
Crystal size	4×4×3 mm^3
Laser	
Power	10 W
Wavelength	514 nm
Pulse width	20 μs
Repetition	1 kHz

7 Experimental results

After these optimizations, an experiment to polarize protons was performed under the conditions summarized in Table 2. The Ar-ion laser was operated in the single-line mode. The average laser power after pulsing was 200 mW. Just after laser irradiation, the magnetic field was swept from −3.5 to +3.5 mT with a rate of 0.47 mT/μs using a field modulation coil while simultaneously applying a microwave pulse to the target crystal. Figure 17 shows the time sequence of laser irradiation, field sweep, and microwave irradiation.

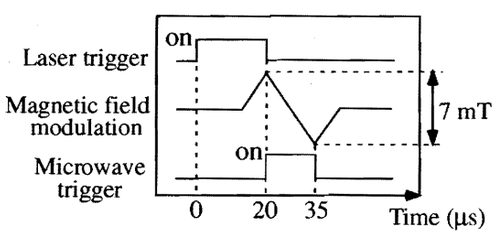

Fig. 17. Time sequence of laser irradiation, field sweep, and microwave irradiation.

Figure 18 shows the result of the proton polarization as a function of time in the buildup process. A proton polarization of 36.8±4.2% was achieved. By fitting the data, the estimated extrapolated maximum polarization is 39.3±4.5%. The relative uncertainty in the proton polarization is 11%, which is mainly due to the uncertainty in determining the NMR signal amplitude in TE. The present proton polarization is comparable to that obtained with the dye laser of 600 nm by Iinuma *et al.* They obtained a 32% polarization with a naphthalene crystal of 3×2×5 mm^3 [10]. Note that the maximum absorption of pentacene occurs at 600 nm (see Fig. 10). The present investigation clearly demonstrates that an Ar-ion laser is a feasible substitute for the dye laser.

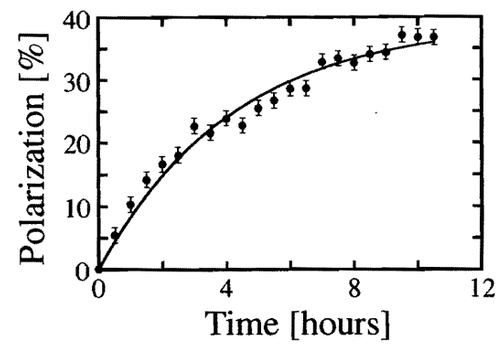

Fig. 18. Proton polarization as a function of time.

We also measured the relaxation time of proton polarization to confirm the quality of the crystal fabrication. The measurements were conducted in 0.3 T at 100 K by observing the decrease in the NMR amplitude as a function of time using a weak RF pulse as shown in Fig. 19. The relaxation time was 23.6±0.7 hours. This result is comparable to the relaxation time of ~20 hours for a pure naphthalene crystal measured at 94 mT [15]. Although the relaxation time tends to be longer in a high magnetic field, the target crystal appears to be successfully grown considering the dopant effect. The quality of crystal fabrication is sufficient for our application.

8 Summary

The design and operation of a proton polarizing system for the $\vec{p}$-RI scattering experiments was described. A proton polarization of 36.8±4.2% was achieved in a magnetic field of 0.3 T at a temperature of 100 K. It was shown that the Ar-ion laser is a suitable light source for a high proton polarization. Since an Ar-ion laser demands

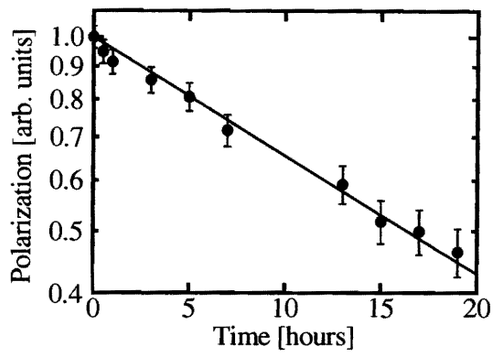

Fig. 19. Decrease in NMR amplitude as a function of time. This measurement was conducted without laser irradiation.

minimum maintenance and has a lifetime greater than 3000 hours, it is well suited for $\vec{p}$-RI scattering experiments that last for a week and requires a stable and continuous light source.

We also presented a method for fabricating a target crystal. To confirm the fabrication quality, the relaxation time of a proton polarization was measured and found to be 23.6±0.7 hours, which is comparable to that for a pure naphthalene crystal. This result shows that our refinement and crystallization processes are appropriate for fabricating a target crystal.

The present proton polarizing system was not optimized as a polarized proton target. Some equipment, including the target crystal, the NMR coil, and the magnetic field modulation coil, should be enlarged to cope with the large spot size of RI beams. This enlarged system has already been constructed based on the present study and was used for the first time in an experiment with a radioactive ^{6}He beam [17]. The target system and the results of the experiment will be presented elsewhere.

Acknowledgements

The authors would like to thank I. Tanihata and T. Suda for their continuous support of this study. They are also grateful to M. Iinuma and K. Takeda for their valuable advise and helpful discussions. We would like to also thank Y. Sekido at Ohyo Koken Kogyo Co., Ltd. for measuring the temperature distribution in the glass vessel used for crystallization. This work is supported by a Grant-in-Aid for Scientific Research No. 15740139 of the Ministry of Education, Culture, Sports, Science, and Technology of Japan.

References

[1] I. Tanihata, Nucl. Phys. A616 (1997) 56c.

[2] D. G. Crabb and W. Meyer, Annu. Rev. Nucl. Part. Sci. 47 (1997) 67.

[3] St. Goertz, W. Meyer, and G. Reicherz, Progr. Part. Nucl. Phys. 49 (2002) 403.

[4] A. Henstra, T.-S. Lin, J. Schmidt, and W. Th. Wenckebach, Chem. Phys. Lett. 165 (1990) 6.

[5] S. S. Kim and S. I. Weissman, Rev. Chem. Intermed. 3 (1979) 107.

[6] D. J. Sloop, H.-L. Yu, T.-S. Lin, and S. I. Weissman, J. Chem. Phys. 75 (1981) 3746.

[7] A. Henstra, P. Dirksen, and W. Th. Wenckebach, Phys. Lett. A134 (1988) 134.

[8] M. Iinuma, I. Shaké, R. Takizawa, M. Daigo, H. M. Shimizu, Y. Takahashi, A. Masaike, and T. Yabuzaki, Phys. Lett. A208 (1995) 251.

[9] K. Takeda, K. Takegoshi, and T. Terao, Chem. Phys. Lett. 345 (2001) 166.

[10] M. Iinuma, Y. Takahashi, I. Shaké, M. Oda, A. Masaike, T. Yabuzaki, and H. M. Shimizu, Phys. Rev. Lett. 84 (2000) 171.

[11] V. S. Antonov and K. L. Hohla, Appl. Phys. B32 (1983) 9.

[12] W. R. Lambert and A. H. Zewail, Chem. Phys. Lett. 69 (1980) 270.

[13] H. de Vries and D. A. Wiersma, J. Chem, Phys. Lett. 70 (1979) 5807.

[14] M. Iinuma, Ph. D. Thesis, Kyoto University (1997).

[15] J. U. von Schuetz and H. C. Wolf, Z. Naturforsch 27 (1972) 42.

[16] D. E. Cooper, R. W. Olson, and M. D. Fayer, J. Chem. Phys. 72 (1980) 2332.

[17] M. Hatano, Ph. D. Thesis, University of Tokyo (2004).